Int. J. Electrochem. Sci., 10 **(2015)** 3414 - 3430

International Journal of ELECTROCHEMICAL SCIENCE
www.electrochemsci.org

Comparative Supercapacitive Properties of Asymmetry Two Electrode Coin Type Supercapacitor Cells made from MWCNTS/Cobalt Oxide and MWCNTs/Iron Oxide Nanocomposite

Abolanle S. Adekunle[1,2], *Bolade O. Agboola*[3,*], *Kenneth I. Ozoemena*[4,5], *Eno E. Ebenso*[2], *John A.O. Oyekunle*[1], *Oluwafemi S. Oluwatobi*[6], *Joel N. Lekitima*[5]

[1]Department of Chemistry, Obafemi Awolowo University, Ile-Ife, Nigeria
[2]Department of Chemistry, School of Mathematical and Physical Sciences, Faculty of Agriculture, Science and Technology, North-West University (Mafikeng Campus), Private Bag X2046, Mmabatho 2735, South Africa
[3]Department of Petroleum Chemistry and Engineering, American University of Nigeria, Yola, Nigeria
[4]Energy & Processes Unit, Materials Science and Manufacturing, Council for Scientific and Industrial Research (CSIR), Pretoria 0001, South Africa
[5]Department of Chemistry, University of Pretoria, Pretoria 0002, South Africa
[6]Department of Chemistry, Cape-Peninsula University of Technology, P. O Box 652, Cape Town, 8000, Western Cape, South Africa.
[*]E-mail: bolade.agboola@aun.edu.ng, bolade_agboola@yahoo.co.uk

Received: 25 October 2014 / *Accepted:* 17 January 2015 / *Published:* 24 February 2015

Supercapacitive properties of synthesized metal oxide nanoparticles (MO) vis a vis iron oxides (Fe_2O_3) and cobalt oxide (Co_3O_4) nanoparticles integrated with multi-walled carbon nanotubes (MWCNT) in a two-electrode coin cell type asymmetry supercapacitor assembly was investigated. The synthesised MO and nanocomposite films were characterised using techniques such as transmission electron microscopy (TEM), scan electron microscopy (SEM), electron dispersive X-ray spectroscopy (EDX) and X-ray diffraction spectroscopy (XRD). The supercapacitance of the asymmetry MWCNT-MO based supercapacitor in 1 M H_2SO_4 and 1 M Na_2SO_4 electrolytes was measured using cyclic voltammetry (CV), electrochemical impedance spectroscopy (EIS) and galvanostatic constant current charge-discharge (CD) techniques. The asymmetry supercapacitors MWCNT-Fe_2O_3|MWCNT and MWCNT-Co_3O_4|MWCNT gave the highest specific capacitance (*SC*) values of 439.94 $mFcm^{-2}$ (or 64.74 Fg^{-1}) and 425.83 $mFcm^{-2}$ (or 45.79 Fg^{-1}) respectively in 1 M H_2SO_4 using charge-discharge technique. Results obtained from charge-discharge experiment are much higher compared with those obtained using the CV technique since it is the most reliable and accurate method. The values compared favorably and higher compared to those reported in literature using similar technique. MWCNT-Fe_2O_3|MWCNT cell gave specific power (*SP*) and specific energy (*SE*) of 19.31 Wkg^{-1} and

2.68 $WhKg^{-1}$ respectively in 1 M H_2SO_4, while the energy deliverable efficiency (η/%) of the cell is 99.6 and 91.3% in 1 M H_2SO_4 and 1 M Na_2SO_4 respectively.

Keywords: MWCNT-iron oxide, MWCNT-cobalt oxide nanocomposites; Electrochemical Impedance; Galvanostatic charge-discharge; Asymmetry assembly.

1. INTRODUCTION

Electrochemical redox supercapacitors consist of electroactive materials with several oxidation states. Their high capacitance and energy characteristics have been investigated [1]. There is no doubt that the present world drastic increase in population and industrialisation, plus the increasing human demands in digital communication, electric vehicles, and other devices that require electrical energy at high power levels in relatively short pulses have prompted considerable interest in this type of supercapacitor system. Several materials such as the redox active metals, transition metal oxides [2-4] and conducting polymers [5] with various oxidation states have been used for this supercapacitor type.

Eventhough, RuO_2 is well known as a good metal oxide in supercapacitors because of its high specific capacitance values (740 Fg^{-1}) [6], from a three electrode system. However, its application is limited because of disadvantages such as the high cost and toxic nature [6]. In the quest for alternative sources, researchers have explored the charge storage properties of different materials such as anhydrous cobalt–nickel oxides [7], MnO_2 or MnOx [8, 9], NiO [10], Co_3O_4 [11], and Fe_3O_4 [12] as inexpensive alternatives to RuO_2. Thus, the need for other transition metal and metal oxides and their composites which are user- and environmentally friendly, providing a sufficiently high power and energy, and can be made available at a relatively cheap price for commercial application cannot be overemphasised.

Since it was reported that the hybrid of an electric double layer system and a Faradaic pseudocapacitive system could be a good candidate for a supercapacitor with high specific capacitance and energy density [13], therefore, recent work was focused on the supercapacitive properties of carbon nanotubes-metal oxide or carbon nanotubes polymer films as potential material for application in supercapacitors. For example, electro synthesized metal (Ni, Fe, Co) oxide films on single-walled carbon nanotube platforms and their supercapacitance in acidic and neutral pH media have been reported [14]. The nanocomposite gave specific capacitance values that compared favourably and higher than those reported in literature. Similarly, the supercapacitive behavior of chemically synthesized metal (Ni, Fe, Co) oxide and multi-walled carbon nanotube nanocomposite in acidic and neutral pH media have been studied [15]. Other related studies include the Supercapacitiveproperties of symmetry and the asymmetry two electrodes coin type supercapacitor cells made from MWCNTS/Nickel oxide Nanocomposite [16], supercapacitive properties of electrochemically grown composite films of multiwalled carbon nanotubes (MWNT) and polypyrrole (PPy), a conducting polymer [17], supercapacitive properties ofnickel (II) octa [(3,5-bicarboxylate)-phenoxy] phthalocyanine integrated with functionalised single-walled carbon nanotubes (SWCNT-phenylamine)

in 0.5 M Na_2SO_4 [18], and the supercapacitive properties of nickel(II) tetra-aminophthalocyanine (NiTAPc)/multi-walled carbon nanotube (MWCNT) nanocomposite films in 1 M H_2SO_4 [19].

In this study, the supercapacitive properties of the chemically synthesised iron and cobalt oxides nanoparticles integrated with MWCNT in acidic and neutral medium using a two-electrode system in a coin type supercapacitor cell were compared. The work was carried out to provide information for this type of supercapacitor cell in acidic medium which are mostly scarce in literature since most studies are carried out in an alkaline medium. The results obtained demonstrated that iron oxide/MWCNT nanocomposite gave better capacitance values in both media compared with cobalt oxide/MWCNT nanocomposite, and the results obtained for both metal oxides in this study compared favourably with other studies earlier reported in literatures. Asymmetry assembly is chosen in this work since previous work in our group using MWCNT-NiO showed that the asymmetry electrode system gave better capacitive properties compared to the symmetry electrode system [16].

2. EXPERIMENTAL

2.1 Materials and reagents

Aluminium foil current-collector of 12 mm in diameter, binder (polyvinylidene fluoride, N-methylpyrrolidione (NMP) solvent, two-electrode coin-type cells (CR 2032) with steel foil, multi-walled carbon nanotubes (MWCNTs), obtained from Aldrich, and acid-digested using the known procedure [20], $Co(NO_3)_2.6H_2O$, $Fe(NO_3)_3.9H_2O$, H_2SO_4 and Na_2SO_4 were obtained from Sigma-Aldrich chemicals. Ultra pure water of resistivity 18.2 MΩcm was obtained from a Milli-Q Water System (Millipore Corp., Bedford, MA, USA) and used throughout for the preparation of solutions. A phosphate buffer solution (PBS, pH 7.0) was prepared with appropriate amounts of K_2HPO_4 and KH_2PO_4, and the pH adjusted with 0.1 M H_3PO_4 or NaOH. All electrochemical experiments were performed with nitrogen-saturated PBS. All other reagents were of analytical grades and were used as received from the suppliers without further purification.

2.2 Syntheses of cobalt and iron oxide nanoparticles

Cobalt oxide nanoparticles were prepared using the method described by Yao et al [21]. A known weight (3.0 g) of $Co(NO_3)_2.6H_2O$ was dissolved into 100 mL of isopropyl alcohol-water (1:1, v/v) solution in a three-necked round-bottom flask. Then appropriate amount of isopropyl alcohol-ammonia solution (45-50 mL) was added into the solution and aged for hours to ensure complete precipitation. The precipitate was filtered and dried under vacuum at 70 ^oC. The Co_3O_4 was finally obtained by calcining the $Co(OH)_2$ precursor at 500 ^oC in Ar for 2 h.

The maghemite (Fe_2O_3) nanoparticles were synthesized by the method described by Sun et al. [22]. First, Magnetite (Fe_3O_4) nanoparticles were synthesized according to the method proposed by Qu et al [23]. Briefly, 3 mL $Fe(NO_3).9H_2O$ (2 M dissolved in 2 M HCl) was added to 10.33 mL double distilled water, and 2 mL Na_2SO_3 (1 M) was added to the former solution drop wise in 1 min under

magnetic stirring. Just after mixing the solutions, the colour of the solution changed from light yellow to red, indicating complex ions formed between the Fe^{3+} and SO_3^{2-}. When the colour of the solution turned back from red to yellow, it was added to 80 mL $NH_3.H_2O$ solution (0.85 M) under vigorous stirring. A black precipitate quickly formed, which was allowed to crystallize completely for another 30 min under magnetic stirring. The precipitate was washed with deoxygenated water by magnetic decantation until the pH of the suspension was less than 7.5. The suspension was dried under vacuum at ambient temperature until it turned to black powder. The black precipitate obtained above was diluted to a volume of 84 mL with a mass concentration of 3 mg/mL forming a suspension. The temperature of the suspension was raised to 90 ^oC in 5 min, and was stirred for 60 min at about 100 ^oC. The colour of the suspension slowly changed from black to reddish-brown and the suspension became clear and transparent. The reddish-brown solution was washed with water by magnetic decantation four times. It was then dried to a powdery solid in the oven at 70 ^oC. The synthesised MO nanoparticles were characterised using spectroscopic and microscopic techniques.

2.3 Equipment and Procedure

High resolution field emission scanning electron microscopy (HRSEM) images were obtained with Zeiss Ultra Plus Oberkochem (Germany). Transmission electron microscopy (TEM) experiment was performed using a Model JEOL JEM-2100F field emission transmission electron microscope, Tokyo (Japan) while the energy dispersive X-ray spectra were obtained from NORAN VANTAGE (USA). The XRD analysis was done using a back loading preparation method. The sample was analysed using a PANalyticalX'Pert Pro powder diffractometer (Netherland) with X'Celerator detector and variable divergence- and receiving slits with Fe filtered Co-Kα radiation. Electrochemical experiments were carried out using an Autolab Potentiostat PGSTAT 302 (Eco Chemie, Utrecht, The Netherlands) driven by the GPES software version 4.9. Electrochemical impedance spectroscopy (EIS) measurements were performed with Autolab Frequency Response Analyser (FRA) software between 10 mHz and 100 kHz using a 5 mV rms sinusoidal modulation in the electrolyte solutions at 0.55 and 0.75 V vs. Ag|AgCl, sat'd KCl). ISE ORION meter, model 420A, was used for pH measurements. Experiments were performed at 25±1 °C.

2.4 Electrode Preparation: Coin type cell assembly

The electrochemical performances of the prepared powder of MWCNT-MO (i.e, MWCNT-Co_3O_4 and MWCNT-Fe_2O_3) nanocomposites were investigated using two-electrode coin-type cells (CR 2032) with steel foil as reference electrode. The working electrode was assembled by coating the slurry of the MWCNT-MO on an aluminium foil current-collector of 12 mm in diameter. The mixture composed of 71.4 wt % active material, 14.3 wt % functionalised MWCNT and 14.3 wt % binder (polyvinylidene fluoride) in an N-methylpyrrolidione (NMP) solvent. After drying in an oven at 80^oC for 2 h, the electrodes were pressed under a pressure of 7 MPa for 1 min. The weight of the active materials was determined by weighing the Al foil before and after pressing the powders. The

supercapacitive behaviour was investigated in both acidic (1 M H_2SO_4) and neutral (1 M Na_2SO_4) electrolytes. In the asymmetry assembly, the working electrode (MWCNT-MO) was used as the positive electrode while the MWCNT alone was used as the negative electrode. The electrodes were soaked in the electrolyte for about 10 mins before assembled in the coin cells. A polypropylene (PP) film (Cellgard 2400) was used as the separator. Scheme 1 represents the coin type cell assembly.

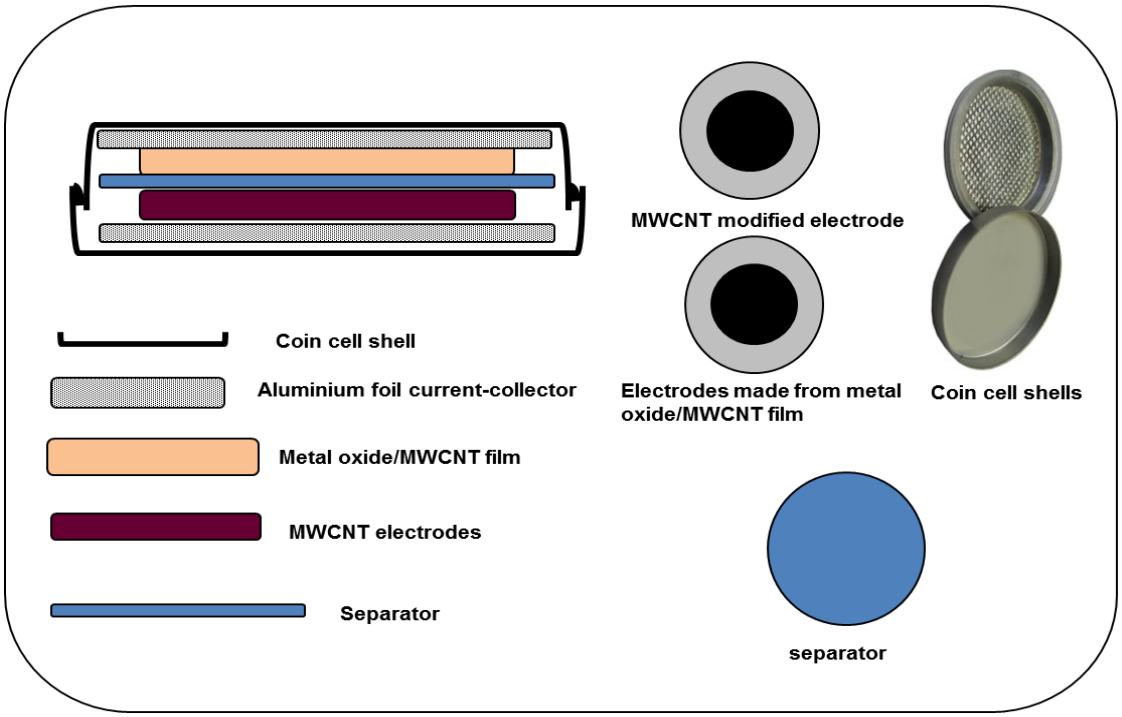

Scheme 1. A coin type two electrode cell made from MWCNT/MO nanocomposite film and MWCNT film.

3. RESULTS AND DISCUSSION

3.1 Comparative FETEM, HRSEM, EDX and XRD studies

The TEM and HRSEM images of the MWCNT-Co_3O_4 and MWCNT-Fe_2O_3 are presented in Fig. 1a-d. The TEM (Fig. 1a) and the SEM (Fig. 1c) images of the Fe_2O_3 nanoparticles showed crystalline particles, evenly distributed along the length of the carbon nanotubes, made possible by ionic interaction between the metal ions and the COO^- charge of the functionalised MWCNTs. The particle diameter is in the range of 10 - 30 nm from the TEM pictures. The reported particle sizes were obtained after calibrating the scale of the TEM image using UTHSCSA image tool for windows version 3.0. The Co_3O_4 also form nano-crystals which are aggregated at one point or the other along the MWCNT (Fig. 1b) and represented as nano-stars by the SEM picture in Fig. 1d. The particle diameter is in the range of 10 - 30 nm from the TEM pictures. In each case, the MWCNT provided

porous and large surface area for the metal oxide to be distributed thus providing them a large coverage on electrode surface for charge storage.

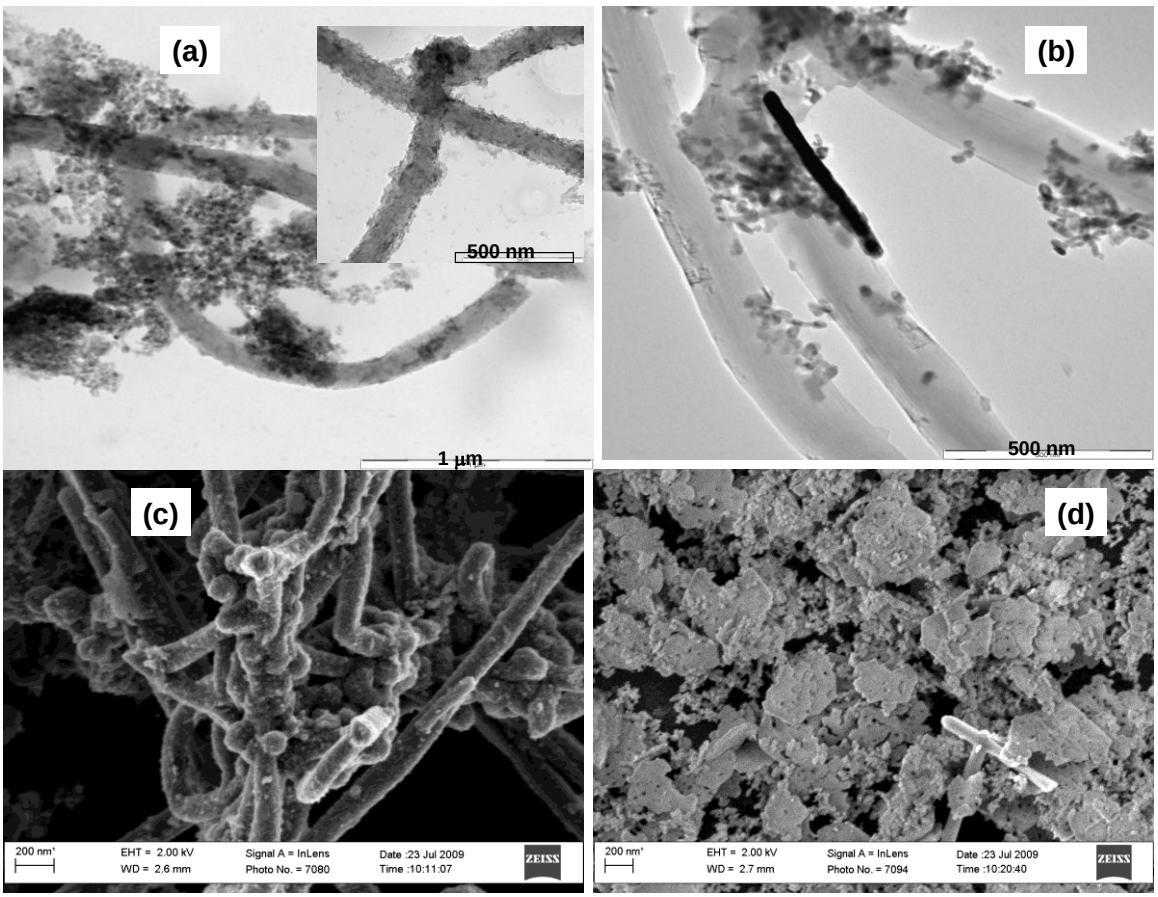

Figure 1. FETEM images of (a) MWCNT-Fe_2O_3, (b) MWCNT-Co_3O_4nanocomposite. (c) and (d) are their respective HRSEM images.

Fig. 2 is the EDX profile of the prepared MWCNT-Co_3O_4 and MWCNT-Fe_2O_3 nanocomposite films. The prominent Co peak in (a) and Fe peak in (b), and the very intense and conspicuous oxygen peak in both cases confirmed the successful synthesis of the oxide form of these metals. The carbon peaks in both (a) and (b) are attributed to the carbon of the MWCNT.

The XRD spectra of the chemically synthesised cobalt and iron oxides are represented in Figure 3a and 3b. From their characteristic peaks at 2θ, and the corresponding miller indices, the oxides are identified as Co_3O_4 and Fe_2O_3 respectively [15], while the average crystal size of the particles were calculated to be ~ 22.8 nm (Co_3O_4) and 10.3 nm (Fe_2O_3) using the Debye-Scherrer formula [15]. The values agreed within the range of the MO nanoparticles sizes reported for the TEM above.

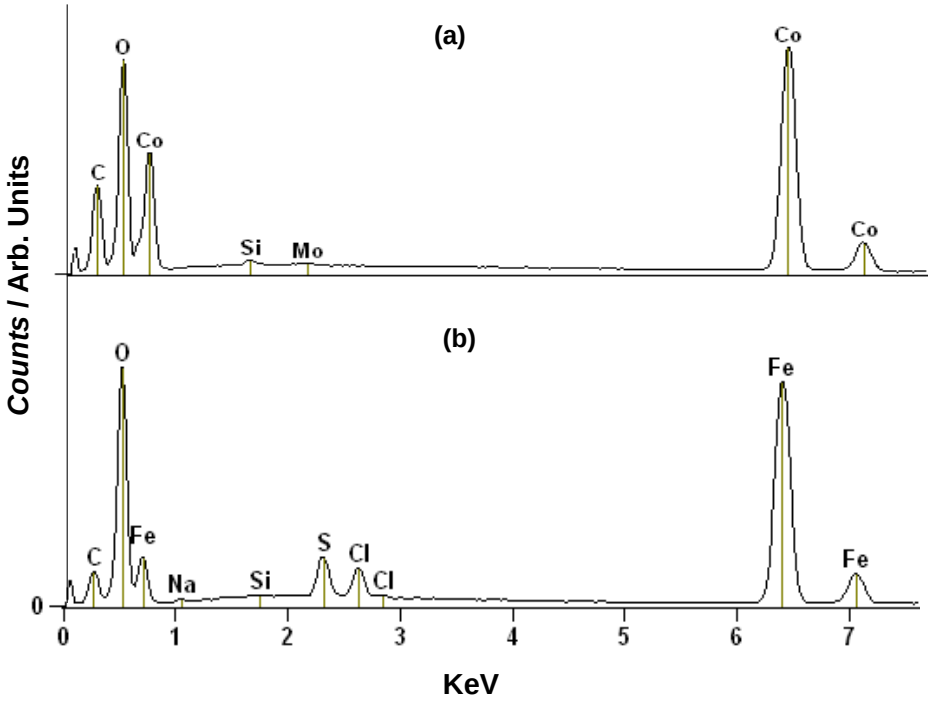

Figure 2. EDX spectra of (a) MWCNT-Co_3O_4 and (b) MWCNT- Fe_2O_3 nanocomposite.

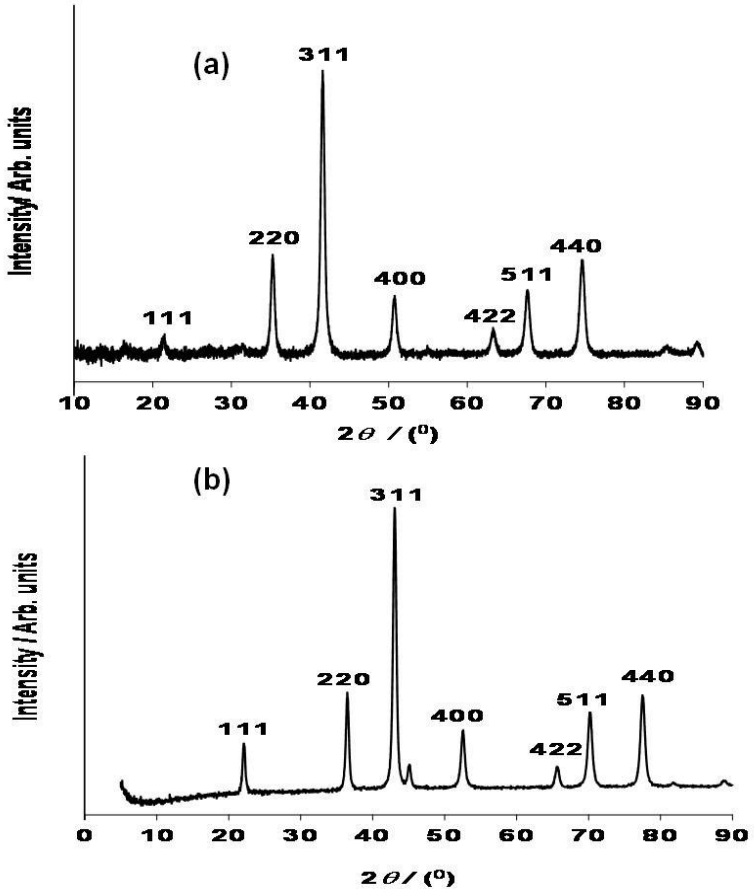

Figure 3. XRD spectra of the synthesised (a) Co_3O_4 and (b) Fe_2O_3nanoparticles.

3.2 Comparative Cyclic Voltammetric Experiments

Comparative cyclic voltammetric experiments of the two coin cell based supercapacitors

Fig. 4 presents the cyclic voltammograms for the asymmetry MWCNT-Fe_2O_3|MWCNT and MWCNT-Co_3O_4|MWCNT based supercapacitors in 1 M H_2SO_4 and 1 M Na_2SO_4 respectively at scan rate of 25 mVs^{-1}. At this scan rate, all the curves exhibited high capacitive currents in both electrolytes especially the MWCNT-Fe_2O_3|MWCNT cell (Figs. 4a and b).

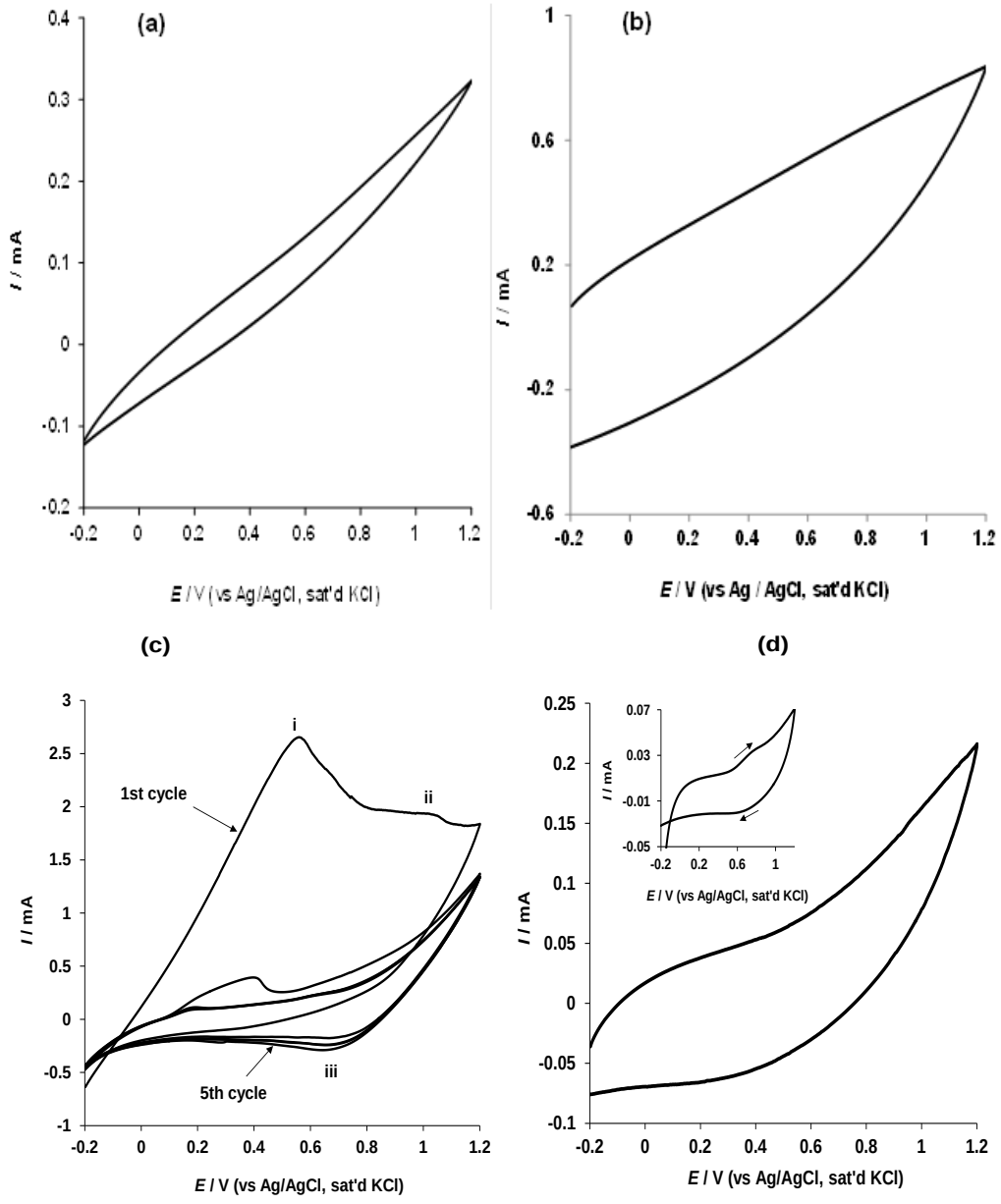

Figure 4. Cyclic voltammograms obtained for the asymmetry (a) and (b) MWCNT-Fe_2O_3|MWCNT supercapacitor (two-electrode cell) and (c) and (d) MWCNT-Co_3O_4|MWCNT based supercapacitors (two-electrode cell) in 1 M H_2SO_4 and 1 M Na_2SO_4 aqueous electrolyte respectively at scan rate of 25 mV s^{-1}. Inset in Fig. 4d is the cyclic voltammograms obtained for the MWCNT-CO_3O_4|MWCNT supercapacitor in Na_2SO_4 electrolyte showing cobalt redox process at scan rate 5 mVs^{-1}.

For the asymmetry based MWCNT-Fe_2O_3|MWCNT supercapacitor, no Fe(II)/Fe(III) redox peaks in both electrolytes was observed as expected for all the scan rate studied (Figs. 4a and b). This could probably be due to very fast faradaic process at the electrode indicating the dominance of pseudocapacitance over double-layer capacitance process. However, MWCNT-Co_3O_4|MWCNT based supercapacitor showed redox peaks at 25 mVs^{-1} in H_2SO_4 which disappeared after subsequent cycles (Fig. 4c). Similar redox process was observed at 5 mVs^{-1} for the MWCNT-CO_3O_4|MWCNT supercapacitor in Na_2SO_4 (inset in Fig. 4d). The anodic peak E_a ~ 0.56 V at position (i) (Fig. 4c) could be attributed to Co(II)/Co(III) process though was observed at higher potential (0.68 V) for EPPGE-SWCNT-CoO modified electrode in phosphate buffer (pH 7.0) [24]. The second anodic peak E_a ~ 1.04 V at point (ii) is due to CoOOH formation from oxidation of $Co(OH)_2$ or Co_3O_4 according to the equations (1) and (2) below [24, 25].

$$Co(OH)_2 + OH^- \longrightarrow CoOOH + H_2O + e^- \quad (1)$$

$$Co_3O_4 + H_2O + OH^- \longrightarrow 3CoOOH + e^- \quad (2)$$

In a reported related study, peak > 1.0 V (vs. Ag/AgCl) has also been attributed to Co_2O_3/Co_3O_4 process [26]. The cathodic peak E_c ~ 0.65 V at position (iii) is attributed to the reduction of CoOOH to $Co(OH)_2$ or Co_3O_4. However, the disappearance of both the anodic and cathodic peak after the first and subsequent cycles, and increasing scan rate indicates increasing capacitive behaviour of the asymmetry MWCNT-CO_3O_4|MWCNT based supercapacitor.

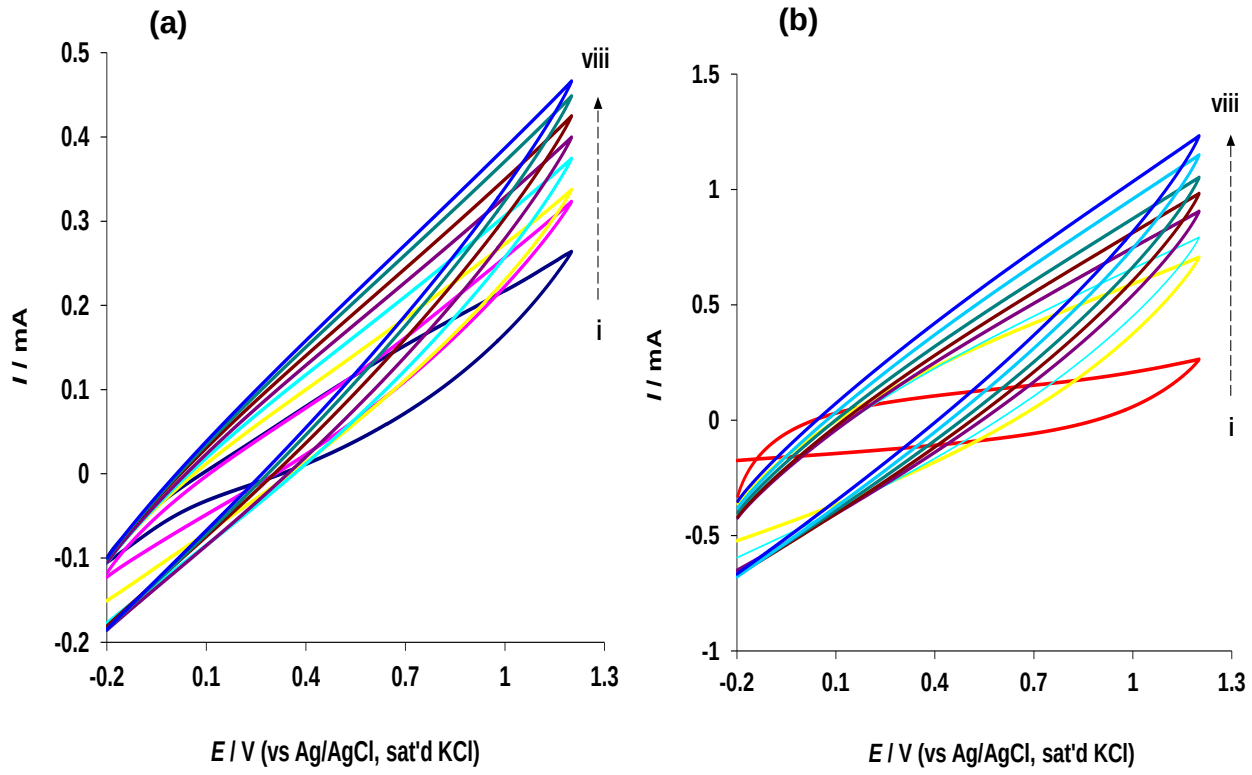

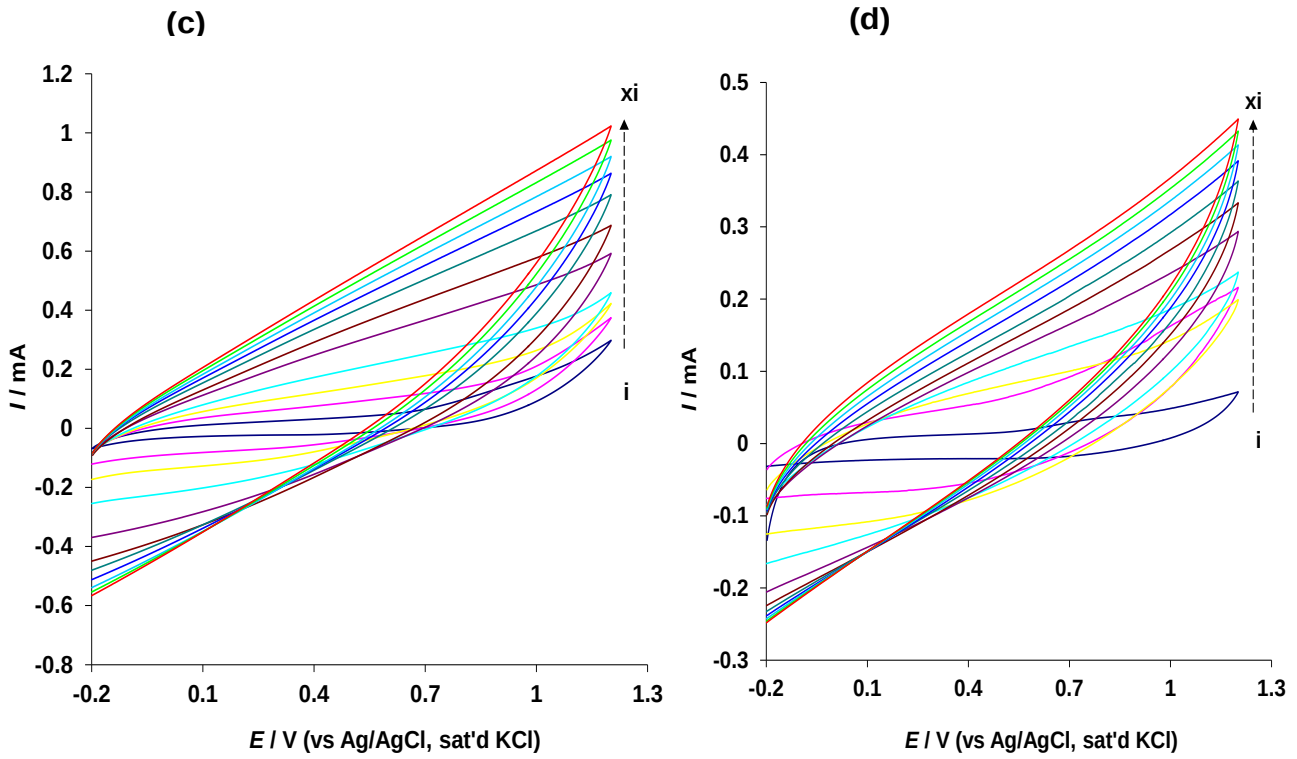

Figure 5. Figures 5a and 5b is the cyclic voltammograms curve obtained for the asymmetry MWCNT-Fe_2O_3|MWCNT in 1 M H_2SO_4 and 1 M Na_2SO_4 aqueous electrolyte respectively at scan rate 5, 25, 100, 200, 300, 400, 600 and 800 mVs^{-1} (i-viii, inner to outer); while Figure 5c and 5d represent the cyclic voltammograms obtained for the asymmetry MWCNT-Co_3O_4|MWCNT based supercapacitor in 1 M H_2SO_4 and 1 M Na_2SO_4 aqueous electrolyte respectively at scan rate 5, 25, 50, 100, 200, 300, 400, 500, 600, 700 and 800 mVs^{-1} (i-xi, inner to outer).

Fig. 5 presents the effect of scan rate on the capacitive behaviour of the supercapacitors. Fig. 5a and 5b is the cyclic voltammograms curve obtained for the asymmetry MWCNT-Fe_2O_3|MWCNT in 1 M H_2SO_4 and 1 M Na_2SO_4 aqueous electrolyte respectively at scan rate 5, 25, 100, 200, 300, 400, 600 and 800 mVs^{-1} (i-viii, inner to outer); while Figure 5c and 5d represent the cyclic voltammograms obtained for the asymmetry MWCNT-Co_3O_4|MWCNT based supercapacitor in 1 M H_2SO_4 and 1 M Na_2SO_4 aqueous electrolyte respectively at scan rate 5, 25, 50, 100, 200, 300, 400, 500, 600, 700 and 800 mVs^{-1} (i-xi, inner to outer).

The asymmetry MWCNT-Co_3O_4|MWCNT based supercapacitor curves tend to be more rectangular than that of MWCNT-Fe_2O_3|MWCNT but lack of perfect rectangular shape for all the curves at the scan rate studied is attributed to the combination of double layer and pseudo-capacitances contributing to the total capacitance [27]. This phenomenon is not unusual especially when redox active materials such as metal oxide are used as part of the composite material for supercapacitors. Similar non perfect rectangular shaped curves are obtained in other studies where there capacitance were obtained using Equation 3 below [27-30].

The specific capacitance (*SC*) was estimated from the cyclic voltammograms using Equation (3) below:

SC_{film} (Fcm^{-2}) = I_{ch}/vA (3)

where I_{ch} is the average charging current, v the scan rate and A is the area of the electrode active material in cm^2. The values obtained are presented in Table 1.0. The equivalent specific capacitance in Fg^{-1} was calculated using Equation (4) [31]:

$$SC\ (\mathrm{Fg^{-1}}) = 2\frac{C}{m} \quad (4)$$

where C is the experimental measured capacitance of the supercapacitor, m is the mass of one composite electrode. The values obtained are represented in parenthesis in Table 1. The capacitance values decreases with increasing scan rate (Table 1). At scan rate of 5 mVs^{-1}, the asymmetry MWCNT-Fe_2O_3|MWCNT supercapacitors exhibited *SC* values of 159.54 and 189.05 mFcm^{-2}, while the asymmetry MWCNT-Co_3O_4|MWCNT supercapacitor exhibited SC values of 50.18 and 36.40 mFcm^{-2} in 1 M H_2SO_4 and 1 M Na_2SO_4 respectively.

Table 1. Specific capacitance (mFcm^{-2}) for the asymmetric MWCNT-Fe_2O_3|MWCNT and MWCNT-Co_3O_4|MWCNT based supercapacitor (two-electrode cell) in 1 M H_2SO_4 and 1 M Na_2SO_4 aqueous electrolyte respectively. Values in parenthesis are the specific capacitance in Fg^{-1}.

Scan rate (mVs^{-1})	Specific capacitance (mFcm^{-2})		Specific capacitance (mFcm^{-2})	
	MWCNT-Fe_2O_3|H_2SO_4|MWCNT	MWCNT-Fe_2O_3|Na_2SO_4|MWCNT	MWCNT-CO_3O_4|H_2SO_4|MWCNT	MWCNT-CO_3O_4|Na_2SO_4|MWCNT
5	159.54 (27.78 Fg^{-1})	189.05 (32.92 Fg^{-1})	50.18 (8.74 Fg^{-1})	36.40 (6.34 Fg^{-1})
25	37.77 (6.58)	104.35 (18.17)	21.38 (3.72)	18.45 (3.21)
50	19.89 (3.46)	34.19 (5.95)	15.85 (2.76)	11.70 (2.04)
100	10.38 (1.81)	17.27 (3.01)	11.94 (2.08)	6.45 (1.12)
200	5.91 (1.03)	10.75 (1.87)	8.28 (1.44)	3.63 (0.63)
300	4.38 (0.76)	8.33 (1.45)	6.33 (1.10)	2.42 (0.45)
400	3.63 (0.63)	7.25 (1.26)	5.03 (0.88)	1.99 (0.35)
500	3.05 (0.53)	6.28 (1.09)	4.41 (0.77)	1.82 (0.32)
600	2.63 (0.46)	5.64 (0.98)	4.05 (0.71)	1.68 (0.29)
700	2.34 (0.41)	5.27 (0.92)	3.75 (0.65)	1.54 (0.27)
800	2.09 (0.36)	9.74 (1.70)	3.51 (0.61)	1.43 (0.25)

Even though the values obtained for the asymmetry MWCNT-Fe_2O_3|MWCNT and MWCNT-Co_3O_4|MWCNT assembly are quite lower compared to 960 $mFcm^{-2}$ reported for asymmetry MWCNT-NiO assembly at the same scan rate (5 mVs^{-1}) in 1 M H_2SO_4 [32], the values were quite higher for MWCNT-Fe_2O_3|MWCNT supercapacitors in both in 1 M H_2SO_4 and 1 M Na_2SO_4 compared with 83 $mFcm^{-2}$ obtained (at the same scan rate) for asymmetric supercapacitor cell assembly based on NiO in 6 M KOH [33]. Also, the 32.92 Fg^{-1} obtained for MWCNT-Fe_2O_3|MWCNT cell in 1 M Na_2SO_4 is greater than 27.67 Fg^{-1} obtained at the same scan rate (5 mVs^{-1}) for asymmetric NiO supercapacitor cell assembly in 6 M KOH electrolyte [33]. The well conducting and mesoporous nature of the functionalised MWCNT which allows more charge flow and storage could be one of the factors responsible for the reasonable high *SC* values obtained for the asymmetry MWCNT-Fe_2O_3|MWCNT based supercapacitors. The low capacitive behaviour of the asymmetry MWCNT-Co_3O_4|MWCNT assembly as indicated by the *SC* values could be due to the method of preparation of this material and electrode decoration, or distribution of the materials on the electrode. For example, the SEM monograph (Fig. 1d) shows particles aggregation forming a nano-star along the MWCNT for the MWCNT-Co_3O_4 electrode. This aggregation may hinder easy charge flow and storage to a large extent in this coin type electrode system. Another factor could be the species form of the synthesized cobalt oxide (Co_3O_4) compared with Fe_2O_3; Fe_2O_3 can readily undergo further oxidation and reduction accordingly, leading to rapid charge flow and storage.

3.3 Electrochemical impedance studies

To further examine the detailed electrical properties or capacitive behaviour of the MWCNT-MO electrodes in the electrolytes, electrochemical impedance spectroscopy (EIS) experiment was conducted at $E_{1/2}$ of 0.55 V vs. Ag|AgCl, sat'd KCl.

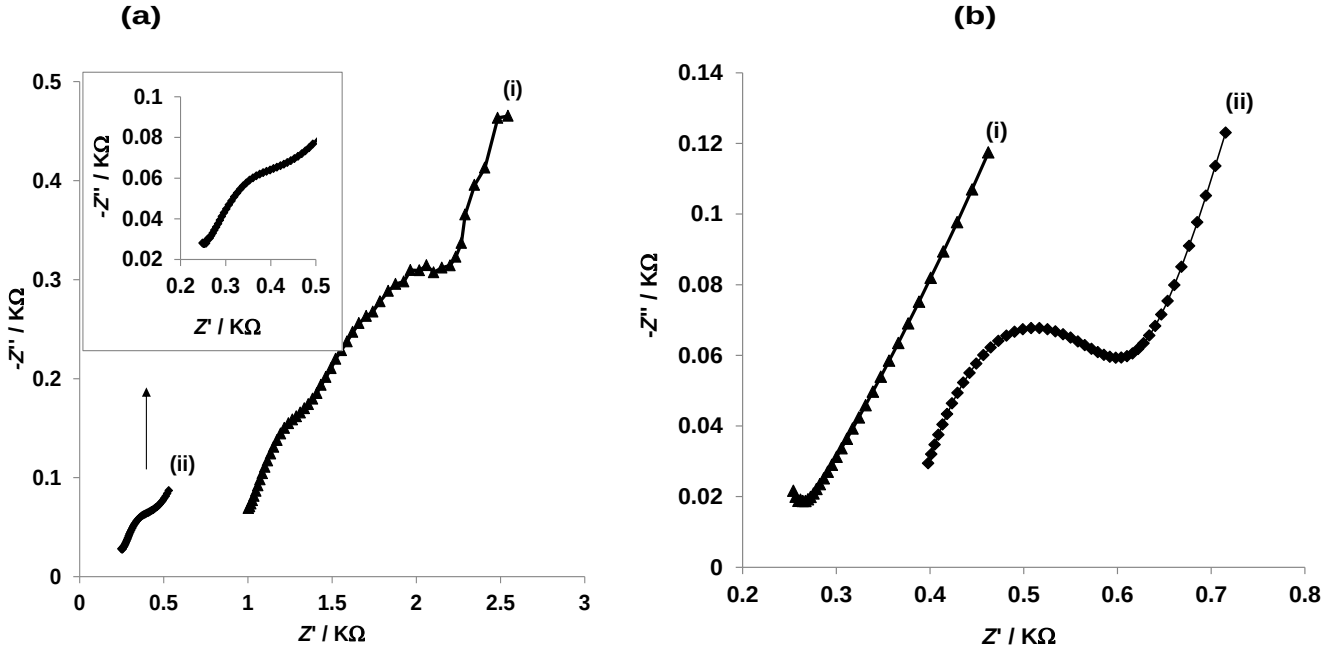

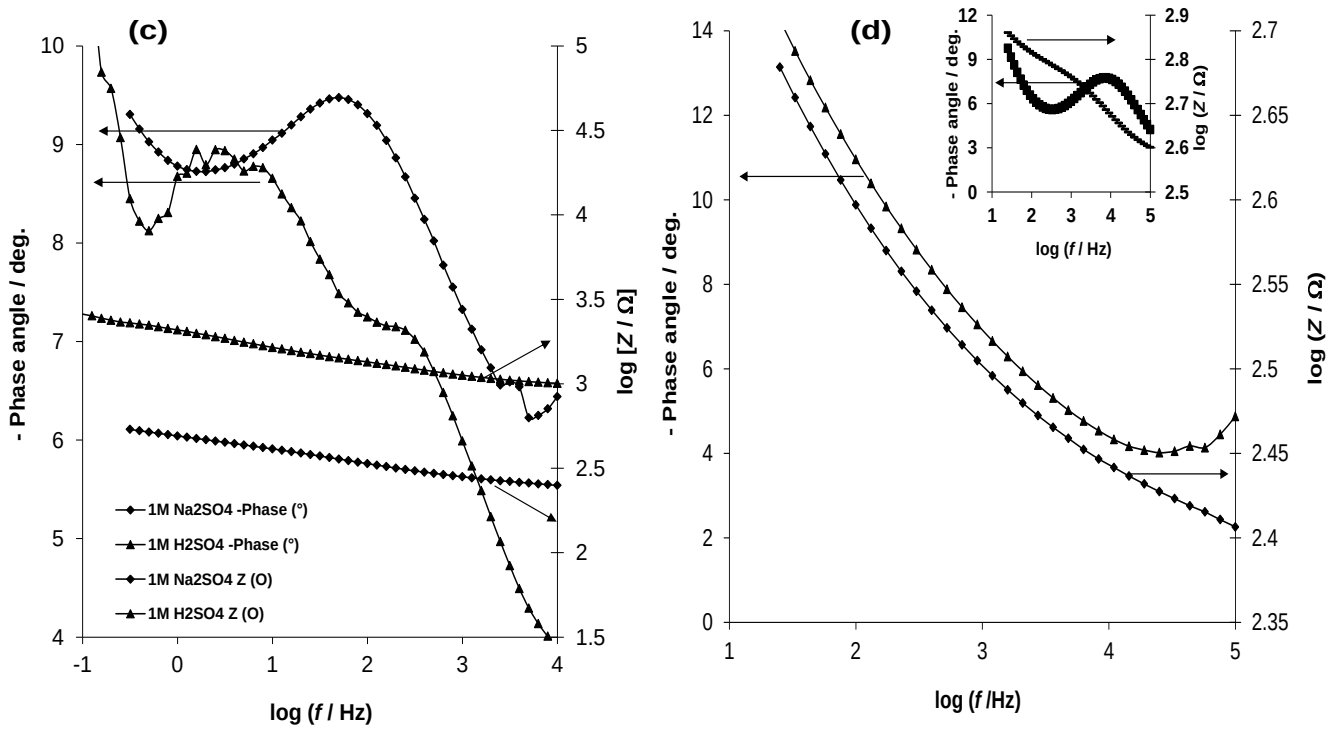

Figure 6. Typical Nyquist plots obtained for the asymmetry (a) MWCNT-Fe_2O_3|MWCNT cell in (i) 1 M H_2SO_4, (ii) 1 M Na_2SO_4 aqueous electrolyte; and (b) MWCNT-Co_3O_4|MWCNT cell in (i) 1 M H_2SO_4, (ii) 1 M Na_2SO_4 aqueous electrolyte at a fixed potential of 0.55 V vs. Ag|AgCl sat'd KCl (c) Plots of (-phase angle, deg) versus log (*f*, Hz); and log (*Z*,□) versus log (*f*, Hz) for MWCNT-Fe_2O_3|MWCNT cell in 1 M H_2SO_4 and 1 M Na_2SO_4 aqueous electrolyte respectively (d) Plots of (-phase angle, deg.) versus log (*f*, Hz); and log (*Z*, □) versus log (*f*, Hz) for MWCNT-Co_3O_4|MWCNT supercapacitor in 1 M H_2SO_4 (inset in 6d represents similar plot in 1 M Na_2SO_4 aqueous electrolyte).

The Nyquist plots obtained for the asymmetry assembly in 1 M H_2SO_4 and 1 M Na_2SO_4 electrolytes respectively are presented in Fig. 6a for MWCNT-Fe_2O_3|MWCNT assembly and Fig. 6b for asymmetry MWCNT-Co_3O_4|MWCNT cell. The Nyquist plots showed a good capacitor-like behaviour with a small diffusion limitation especially for the asymmetry MWCNT-Fe_2O_3|MWCNT in 1 M Na_2SO_4 (Fig. 6a(ii)) and the asymmetry MWCNT-Co_3O_4|MWCNT in 1 M Na_2SO_4 (Fig 6b(ii)). Infact, the large semi-circle (Warburg diffusion) obtained in Nyquist plot in 6b(ii) truly confirmed its low capacitance since there is high resistance to free flow of charges in this supercapacitor.

However, both the MWCNT-Fe_2O_3|MWCNT and MWCNT-Co_3O_4|MWCNT assembly gave smaller arc in 1 M H_2SO_4 (Fig. 6a(i) and 6b(i)), which implies faster diffusion controlled process, low charge transfer resistance, faster charge transport and storage in the supercapacitor, hence, the high SC values recorded in 1 M H_2SO_4 compared with 1 M Na_2SO_4.

Plots of (-phase angle, deg) versus log (*f*, Hz); and log (*Z*, □) versus log (*f*, Hz) for MWCNT-Fe_2O_3|MWCNT and MWCNT-Co_3O_4|MWCNT supercapacitors in the acid and neutral media are presented in Fig. 6c and 6d respectively. Curve of (-phase angle, deg) versus log (*f*, Hz) for MWCNT-Fe_2O_3|MWCNT in 1 M H_2SO_4 was characterised with two phases at phase angles of 9^o and 7^o

respectively (Fig. 6c) suggesting that this cell can readily transfer and store charges at the same time, that is, exhibit both capacitive and pseudocapacitive properties in 1 M H_2SO_4 as compared with a single broad phase at phase angle 9.5^o obtained for the same cell in 1 M Na_2SO_4. MWCNT-Co_3O_4|MWCNT on the other hand gave lower phase angle (7.7^o) at frequency of approximately 4 Hz in 1 M Na_2SO_4, while very rare angle at around 4^o was observed at the same frequency for the electrode in 1 M H_2SO_4 (Fig. 6d). The result further emphasise the favourable transfer and storage of charges by this supercapacitor in H_2SO_4 compared to Na_2SO_4 electrolyte. A phase angle of 90^o is expected for pure and ideal capacitive behaviour, thus the supercapacitors investigated in this study have clearly demonstrated a pseudocapacitive behaviour. Similarly, plots of log (*f*, Hz) versus log (*Z*, Ω) gave slope values less than -1 for both supercapacitors in both the acidic and the neutral media, which is an indicative of high pseudo-capacitive behaviour.

3.4 Comparative galvanostatic charge/discharge experiments

Galvanostatic charge-discharge is the most reliable and accurate method for evaluating the supercapacitance of electrodes. The comparative current charge/discharge experiment of the supercapacitor cell assembly in (a) 1 M H_2SO_4 and (b) 1 M Na_2SO_4 electrolyte solutions at current density of 0.1 mAcm^{-2} was studied at potential range of - 0.2 to 0.8 V to observe the pseudocapacitance arising from the redox reaction at this voltage range. The charge/discharge curve for asymmetry MWCNT-Fe_2O_3|MWCNT and MWCNT-Co_3O_4|MWCNT cell in both electrolytes is presented in Fig. 7 and 8 respectively. The charging and the discharge times are about the same for the different charge/discharge experiment.

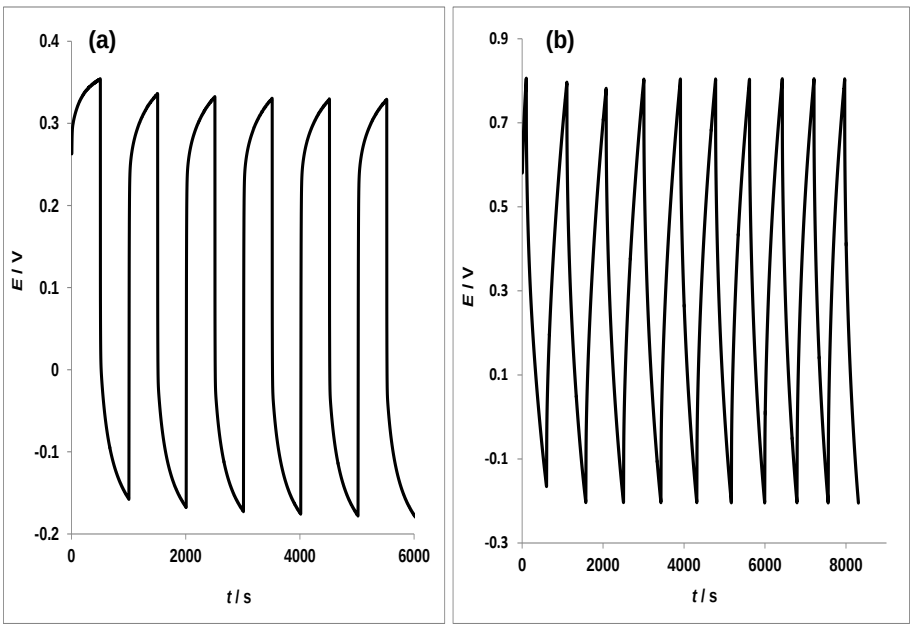

Figure 7. Typical examples of the galvanostatic charge discharge profile for the asymmetry MWCNT-Fe_2O_3|MWCNT supercapacitor (two-electrode cell) in (a) 1 M H_2SO_4 and (b) 1 M Na_2SO_4 aqueous electrolytes, at an applied current density of 0.1 mAcm^{-2}.

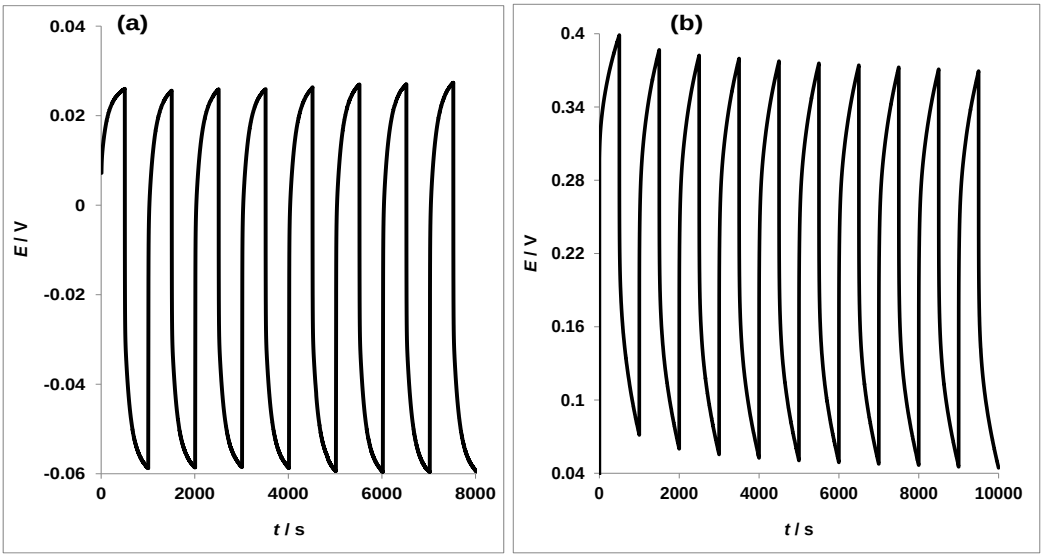

Figure 8. Typical examples of galvanostatic charge discharge profile of the asymmetry MWCNT-Co_3O_4|MWCNT cell supercapacitor (two-electrode cell) in (a) 1 M H_2SO_4 and (b) 1 M Na_2SO_4 aqueous electrolytes, at an applied current density of 0.1 $mAcm^{-2}$.

The specific capacitance of the supercapacitor (*SC*) was calculated using Equations (5) and (6) below [12]:

$$SC\ (Fcm^{-2}) = \frac{I \times \Delta t}{\Delta E \times A} \quad (5)$$

$$SC\ (Fg^{-1}) = \frac{I \times \Delta t}{\Delta E \times m} \quad (6)$$

where I is the discharge current in ampere, Δt is the discharge time in second, ΔE is the discharge voltage in volt, A and m are the area and the mass of the electrode active material in cm^2 or g respectively. The calculated *SC* is 439.94 $mFcm^{-2}$ (or 64.74 Fg^{-1}) and 194.35 $mFcm^{-2}$ (or 16.92 Fg^{-1}) was obtained for the asymmetry MWCNT-Fe_2O_3|MWCNT supercapacitor cell in 1 M H_2SO_4 and 1 M Na_2SO_4 respectively. Similarly, the values 425.83 $mFcm^{-2}$ (45.79 Fg^{-1}) and 135.08 $mFcm^{-2}$ (11.76 Fg^{-1}) were obtained for the MWCNT-Co_3O_4|MWCNT supercapacitor assembly in 1 M H_2SO_4 and 1 M Na_2SO_4 respectively. Results obtained from charge-discharge experiment are much higher compared with those obtained from the CV experiment. The result also indicates that higher *SC* values are obtained in H_2SO_4 than in Na_2SO_4. The higher *SC* values in H_2SO_4 rather than Na_2SO_4 may be attributed to relatively smaller ion size of H^+ in comparison to Na^+, thus easier penetration and mobility of the former in electrode material matrix. But generally, one of the main reasons for the higher value obtained in this study may possibly be due to the stringent conditions adopted in functionalising the MWCNTs with carboxylic, phenolic and ketonic groups which make them more able to enhance ion mobility and storage, and also undergo both non-faradaic (capacitive) and faradaic (pseudocapacitive) reactions.

The *SC* value (64.74 Fg^{-1}) obtained for MWCNT-Fe_2O_3|MWCNT supercapacitor compared favourably with 53.9 Fg^{-1} recorded for the asymmetry MWCNT-NiO|H_2SO_4|MWCNT supercapacitor in H_2SO_4 [32], but higher compared with 37 and 40 Fg^{-1} reported for the symmetry (NiO|KOH|NiO)

and the asymmetry (NiO|KOH|activated carbon) supercapacitors respectively using same technique [33].

The specific power density (*SP*) and specific energy (*SE*) were easily estimated from the discharge process using Equations (7) and (8) [12]:

$$SP\ (\mathrm{WKg^{-1}}) = (I \times \Delta E)/m \quad (7)$$

$$SE\ (\mathrm{WhKg^{-1}}) = (I \times t \times \Delta E)/m \quad (8)$$

All symbols retain their usual meaning. Since the MWCNT-Fe_2O_3|MWCNT cell gave the highest *SC* value, the *SP* and *SE* for the cell in 1 M H_2SO_4 are 19.31 $\mathrm{Wkg^{-1}}$ and 2.68 $\mathrm{WhKg^{-1}}$ respectively. The energy deliverable efficiency (η / %) of the electrode was obtained from Equation (9).

$$\eta\ (\%) = t_d/t_c \times 100 \quad (9)$$

where t_d and t_c are discharge time and charging time, respectively. The energy deliverable efficiency for MWCNT-Fe_2O_3|MWCNT cell in 1 M H_2SO_4 and 1 M Na_2SO_4 is 99.6 and 91.3% respectively.

4. CONCLUSIONS

This study confirmed successful preparation of the MWCNT/MO nanocomposite films for supercapacitor application using characterisation techniques such as HRSEM, FETEM, EDX and XRD. Cyclic voltammetry experiment showed that the asymmetry MWCNT-Fe_2O_3|MWCNT and MWCNT-Co_3O_4|MWCNT supercapacitor cells gave capacitive current with no perfect rectangular shape in both 1 M H_2SO_4 and 1 M Na_2SO_4. Cyclic voltammetry and the electrochemical impedance results suggest both double layer capacitance and pseudocapacitance contributing to the total capacitance in this type of supercapacitors assembly. The galvanostatic charge-discharge technique revealed that the cell MWCNT-Fe_2O_3|MWCNT and MWCNT-Co_3O_4|MWCNT gave the highest specific capacitance (*SC*) values of 439.94 $\mathrm{mFcm^{-2}}$ (or 64.74 $\mathrm{Fg^{-1}}$) and 425.83 $\mathrm{mFcm^{-2}}$ (or 45.79 $\mathrm{Fg^{-1}}$) respectively in 1 M H_2SO_4**.** Results obtained from charge-discharge experiment are much higher compared than those obtained using the CV technique, while the specific capacitance values obtained in this study compared favourably to, and higher than those reported in literature using similar technique. The high capacitive behaviour of the asymmetry MWCNT/MO supercapacitor cells in H_2SO_4 compared to the one in Na_2SO_4 solution has been attributed to easier penetration and mobility of the former in electrode material matrix due to relatively smaller ion size of H^+ in comparison to Na^+, greater diffusion, adsorption and storage capacity along the pores of the MWCNT-MO nanocomposites, and functionalisation of the MWCNTs with carboxylic, phenolic and ketonic groups which make them more able to enhance ion mobility and storage, and also undergo both non-faradaic (capacitive) and faradaic (pseudocapacitive) reactions.

ACKNOWLEDGEMENTS

Authors gratefully acknowledge the following institutions: Council for Scientific and Industrial Research (CSIR) Pretoria, South Africa, University of Pretoria, South Africa, North-West University

(Mafikeng campus) South Africa and American University of Nigeria. A.S. Adekunle is grateful to North-West University for the Postdoctoral Research Fellowship and Obafemi Awolowo University (OAU) Ile-Ife, Nigeria for the leave support.

References

1. T. Shinomiya, V. Gupta, N. Miura, *Electrochim Acta,* 51 (2006) 4412.
2. C-M. Huang, C-H. Hu, K-H. Chang, J-M. Li, Y-F. Li, *J Electrochem Soc,* 156 (2009) A667.
3. P. Ghosh, S. Mahanty, R.N. Basu, *J Electrochem. Soc,* 156 (2009) A677.
4. M.S. Wu, H.H. Hsieh, *Electrochim Acta,* 53 (2008) 3427.
5. V. Srinivasan, J.W. Weidner, *J Electrochem Soc,* 147 (2000) 880.
6. M.D. Ingram, H. Staesche, K.S. Ryder, *J Power Sources,* 129 (2004) 107.
7. C.H. Hu, K.H. Chang, M.C. Lin, Y.T. Wu, *Nano Letters,* 6 (2006) 2690.
8. Z. Fan, J. Chen, K. Cui, F. Sun, Y. Xu, Y. Kuang, *Electrochim Acta,* 52 (2007) 2959.
9. S. Devaraj, N. Munichandraiah, *J Electrochem Soc,* 154 (2007) 80.
10. K.W. Nam, K.B. Kim, *J Electrochem Soc,* 149 (2002) A346.
11. L. Cao, M. Lu, H.L. Li, *J Electrochem Soc* 152 (2005) A871.
12. S.Y. Wang, K.C. Ho, S.L. Kuo, N.L. Wu, *J Electrochem Soc,* 153 (2006) A75.
13. Y.H. Lee, K.H. Ann, J.Y. Lee, S.C., Lim, *Encycl Nanosci Nanotechnol,* 1 (2004) 625.
14. A.S. Adekunle, K.I. Ozoemena, *Electroanalysis,* 23 (2011) 971.
15. A.S. Adekunle, K.I. Ozoemena, B.O. Agboola, *J Solid State Electrochem,*17 (2013) 1311.
16. A.S. Adekunle, B.B. Mamba, B.O. Agboola, O.S. Oluwatobi, K.I. Ozoemena, *Int J Electrochem Sci,* 6 (2011) 4388.
17. M. Hughes, G.Z. Chen, M.S.P. Shaffer, D.J. Fray, A.H. Windle, *Chem Mater,* 14 (2002) 1610.
18. B.O. Agboola, K.I. Ozoemena, *J Power Sources,* 195 (2010) 3841.
19. A.T. Chidembo, K.I. Ozoemena, B.O. Agboola, V. Gupta, G.G. Wildgoose, R.G. Compton, *Energy Environ Sci,* 3 (2010) 228.
20. J.A. Liu, G. Rinzler, H. Dai, J.H. Hanfer, R.K. Bradley, P.J. Boul, A. Lu, T. Iverson, K. Shelimov, C.B. Huffman, F.R. Macias, Y.S. Shon, T.R. Lee, D.T. Colbert, *Science,* 280 (1998) 1253.
21. W.L. Yao, J.L. Wang, J. Yang, G.D. Du, *J Power Sources,* 176 (2008) 369.
22. Y.K. Sun, M. Ma, Y. Zhang, N. Gu, *Colloids and Surfaces A: Physicochem Eng Aspects,* 245 (2004) 15.
23. S. Qu, H. Yang, D. Ren, S. Kan, G. Zou, D. Li, M. Li, *J Colloid Interface Sci,* 215 (1999) 190.
24. A.S. Adekunle, J. Pillay, K.I. Ozoemena, *Electrochim Acta,* 55 (2010) 4319.
25. A. Salimi, R. Hallaj, S. Soltanian, H. Mamkhezri, *Anal Chim Acta,* 594 (2007) 24.
26. S. Sunohara, K. Nishimura, K. Yahikozawa, M. Ueno, *J. Electroanal Chem,* 354 (1993) 161.
27. A.L.M. Reddy, S. Ramaprabhu, *J Phys Chem C,* 111 (2007) 7727.
28. M.S. Wu, H.H. Hsieh, *Electrochim Acta,* 53 (2008) 3427.
29. J. Pillay, K.I. Ozoemena, *Chem Phys Lett,* 441 (2007) 72.
30. M.K. Jang, S.R. Kwang, K. Sanghyo, M.K. Kwang, *J Appl Electrochem,* 39 (2009) 1331.
31. H.Q. Wang, Z.S. Li, Y.G. Huang, Q.Y. Li, X.Y. Wang, *J Mater Chem,* 20 (2010) 3883.
32. A.S. Adekunle, B.B. Mamba, B.O. Agboola, O.S. Oluwatobi, K.I. Ozoemena, *Int J Electrochem Sci,* 6 (2011) 4760.
33. V. Ganesh, S. Pitchumani, V. Lakshminarayanan, *J Power Sources,* 158 (2006) 1523.